Effects of local chemical ordering on the thermal transport in entropy-regulated PbSe-based thermoelectric materials

Shuang Lyu, Ruihuan Cheng, Haiqi Li, Yue Chen*

Department of Mechanical Engineering, The University of Hong Kong, Pokfulam Road, Hong Kong SAR, China

* Corresponding author, e-mail: yuechen@hku.hk

Abstract

Configurational entropy manipulation strategy has been proposed for designing high-performance thermoelectric materials. Understanding the phase stability is essential to regulate the thermal conductivity for optimizing the thermoelectric performance. Herein, the lattice thermal conductivity of PbSe is found to decrease from 1.87 $Wm^{-1}K^{-1}$ to 0.76 $Wm^{-1}K^{-1}$ of $PbSe_{0.5}Te_{0.25}S_{0.25}$, which mainly results from the decreased contribution from the low frequency phonon modes. Moreover, we find local chemical ordering (LCO) in $PbSe_{0.5}Te_{0.25}S_{0.25}$ by conducting hybrid Monte Carlo and molecular dynamics simulations based on our constructed machine-learning interatomic potential. The local chemical ordering can reduce phonon scattering with frequency in 0-2 THz thus enhance thermal conductivity by approximately 14%. This work unfolds the energy favorable structure with LCO in entropy-tailored thermoelectric material, which gives guidance for regulating thermal transport.

Keywords

Local chemical ordering, machine learning potential, lattice thermal conductivity

Direct converting exhaust heat to electricity can be realized by thermoelectric technology, which has triggered arousing interest owing to its potential for improving the overall energy efficiency [1-4]. The thermoelectric performance is measured by a dimensionless figure-of-merit $zT = S^2\sigma T/(k_L + k_e)$, where S, σ, k_L and k_e correspond to the Seebeck coefficient, electrical conductivity, lattice and electronic thermal conductivity, respectively. In addition to band engineering [5,6] for S, σ and k_e optimization to enhance zT, alloying and lattice defects can hinder the propagation of heat-carrying phonons [7-10], leading to a decrease of k_L and an improvement of zT.

Entropy engineering, which can simultaneously realize a stable crystalline structure and a random atomic arrangement by increasing element species, has been proposed as an alternative strategy to optimize thermoelectric performance [1,8,11]. The chemical randomness and atomic size mismatch induced severe lattice distortion can strongly scatter phonons, yielding low k_L [12]. However, instead of a stable random solid-solution phase, the competition between entropy and enthalpy ($\Delta G = \Delta H - T\Delta S$) can lead high/medium entropy alloy systems towards inherent local chemical ordering (LCO), as reported by computational simulations [13-15] and direct experimental observations [16,17]. Whether the LCO also appears in high entropy compositional thermoelectric materials, and the corresponding influences on the thermal transport have not yet been systematically investigated.

In this work, we first constructed an efficient machine-learning neuroevolution potential (NEP) [18] for the Pb-Se-Te-S system based on density functional theory (DFT) calculations. The training dataset for the machine learning interatomic potential includes binary, ternary and quaternary configurations (described in the Supplementary Information), of which the energies and atomic forces were calculated from density functional theory. The graphics processing units molecular dynamics (GPUMD) package [18-20] was adopted to construct the neuroevolution potential. Radial (r_c^R) and angular (r_c^A) cutoffs of 8 Å and 4 Å, respectively, with a basis size of 12 and a batch

size of 1000 were applied, and we used the default weight values for energy loss ($\lambda_e = 1$), force loss ($\lambda_f = 1$) and virial loss ($\lambda_v = 0.1$) during the optimization. To validate the applicability of the NEP to complex atomic environments, we generated a testing set containing 191 different configurations, with details included in the supplementary material.

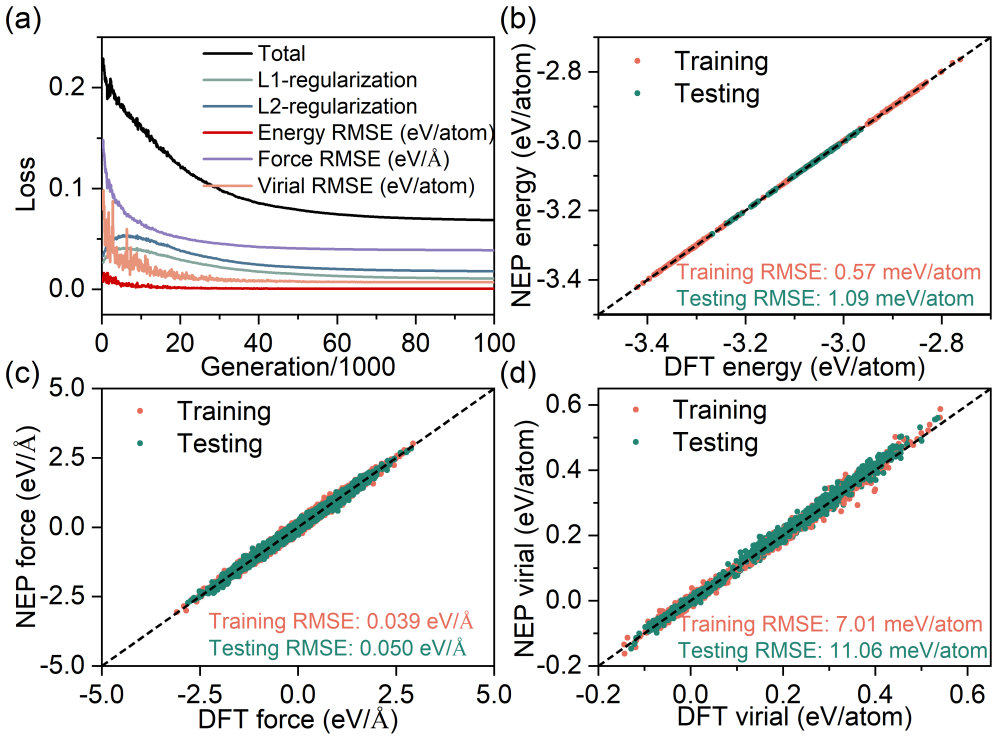

Figure 1. Machine-learning interatomic potential evaluation for the Pb-Se-Te-S system. (a) Loss functions and training root mean square errors (RMSEs) related to the regularization with respect to the training algorithm. Comparisons of the energies (b), atomic forces (c) and virial (d) for the training and testing sets calculated from NEP and DFT. The black dashed lines in (b-d) represent the identity functions that serve as a guide to the eye.

The interatomic potential for the Pb-Se-Te-S system was developed based on the NEP formalism [18]. Figure 1 (a) shows the loss functions and root-mean-square errors (RMSEs) of energies, forces, and virials during the training process. It is found that 100,000 generations are sufficient for the convergence of the training process. Comparisons of the NEP- and DFT-predicted energies, atomic forces, and virials of the training and validation sets are also presented in Figure 1(b-d). The RMSEs for the training and testing configurations are, respectively, 0.57 meV/atom and 1.09

meV/atom for energies, 0.039 eV/Å and 0.050 eV/Å for the atomic forces, and 7.01 meV/atom and 11.06 meV/atom for virials, indicating that the NEP can achieve high accuracy in describing the complex atomic environments. We have also calculated the lattice thermal conductivities of the binary systems PbSe, PbTe, and PbS via homogeneous nonequilibrium MD (HNEMD, as described below); the results are in good agreement with the experimental values, as presented in Figure S1 in supplementary material [21,22].

HNEMD, as implemented in the GPUMD package [23], is a nonequilibrium but homogeneous method because external forces are added and no temperature gradient is generated. Using the developed NEP, we first performed NPT equilibrium at 300 K for 20 ps to obtain the lattice constants. System equilibration was then conducted under NVT ensemble for 100 ps, followed by NVT ensemble simulations to obtain the heat flux, which was subsequently used to calculate the lattice thermal conductivity [23].

$$\kappa(t) = \frac{1}{t}\int_0^t ds \frac{<J_q(s)>_{ne}}{TVF_e} \quad (1)$$

Here, $<J_q(s)>_{ne}$ is the heat current; T, V, and F_e are the absolute temperature, system volume, and the external driving force, respectively.

The nonequilibrium heat current can be resolved in the frequency domain [23]. The steady-state time correlation function can be calculated by:

$$\boldsymbol{K}(t) = \sum_i \sum_{j\neq i} r_{ij}(0) < \frac{\partial U_j}{\partial \boldsymbol{r}_{ji}}(0) \cdot \frac{\boldsymbol{p}_i(t)}{m_i} >_{ne} \quad (2)$$

which reduces to the nonequilibrium heat current when $t = 0$. Then the Fourier transform is defined as:

$$\widetilde{\boldsymbol{K}}(\omega) = \int_{-\infty}^{\infty} dt e^{i\omega t} \boldsymbol{K}(t) \quad (3)$$

The spectral thermal conductivity can then be obtained:

$$\boldsymbol{\kappa}(\omega) = \frac{2\widetilde{\boldsymbol{K}}(\omega)}{TVF_e} \quad (4)$$

where U_i, $\boldsymbol{p}_i$, and m_i are the potential energy, momentum, and mass of particle i, respectively; $\boldsymbol{r}_{ij} = \boldsymbol{r}_j - \boldsymbol{r}_i$ is the position difference between particle j and i.

During HNEMD simulation, the timestep for integration was set to 1 fs, the driving force was chosen as $F_e = 0.0001$ Å^{-1} (see Figure S2 in supplementary material for the convergence test). We performed 15 independent simulations, each with a production time of 2 ns, to calculate the average thermal conductivity. A total correlation steps of 800, maximum angular frequency of $40/2\pi$ THz, and sample interval of 10 were used for spectral thermal conductivity calculation. The thermal conductivities of all binary PbSe, PbS, PbTe, ternary $PbSe_{0.5}Te_{0.5}$, $PbSe_{0.5}S_{0.5}$, and quaternary $PbSe_{0.5}Te_{0.25}S_{0.25}$ were calculated based on a $17 \times 17 \times 17$ supercell (39304 atoms) to eliminate the size effect (see Figure S3 in supplementary material for the convergence test).

Alloying, a common approach to introduce disorder, is often used to enhance the phonon scattering rates and decrease the lattice thermal conductivity. In addition to the ternary systems $PbSe_{0.5}Te_{0.5}$ and $PbSe_{0.5}S_{0.5}$, we have also randomly substituted 50% of the Se atoms with 25% of Te and 25% of S to form a quaternary system to investigate the entropy effects on the thermal transport properties. The running thermal conductivity $k(t)$ of $PbSe_{0.5}Te_{0.25}S_{0.25}$ as a function of correlation time is shown in Figure 2(a). It is seen that the averaged $k(t)$ (green thick solid line) converges well in the range between 1 and 2 ns. Figure 2 (b) shows the temperature-dependent lattice thermal conductivity k_L of PbSe and the alloyed ternary and quaternary systems obtained from MD simulations. The thermal conductivity of $PbSe_{0.5}S_{0.5}$ is in reasonable agreement with the experimental result [22]. The k_L at 300 K decreases from 1.87 $Wm^{-1}K^{-1}$ for PbSe to 1.25 $Wm^{-1}K^{-1}$ and 0.97 $Wm^{-1}K^{-1}$ when 50% of the Se atoms are replaced by S and Te, respectively. When Se atoms are substituted by 25% Te and 25% S, the k_L of the quaternary system further decreases to 0.76 $Wm^{-1}K^{-1}$. Atomic size differences in these highly disordered systems result in deformed unit cells (lattice distortion), leading to inhomogeneous local force field, which can enhance phonon scattering and be responsible for the reduction of k_L [24-26].

To comprehend the alloying effects on the phonon contribution to the thermal conductivity, we have calculated the spectral thermal conductivity $\kappa(\omega)$ of PbSe, $PbSe_{0.5}Te_{0.5}$, $PbSe_{0.5}S_{0.5}$ and $PbSe_{0.5}Te_{0.25}S_{0.25}$ at 300 K, as shown in Figure 2(c). The phonon contribution to k_L in the frequency range from 0.5 to 2 THz decreases significantly after alloying. From Figure 2 (d), it is evident that there is almost no phonon vibrational mode with frequency higher than 5 THz exists in PbSe and $PbSe_{0.5}Te_{0.5}$, which is consistent with the flat cumulative thermal conductivity in Figure 2(c). Observable high-frequency phonons exist in $PbSe_{0.5}S_{0.5}$ and $PbSe_{0.5}Te_{0.25}S_{0.25}$, suggesting that the addition of light-weight S atoms can enhance the high-frequency phonon contribution to the lattice thermal conductivity.

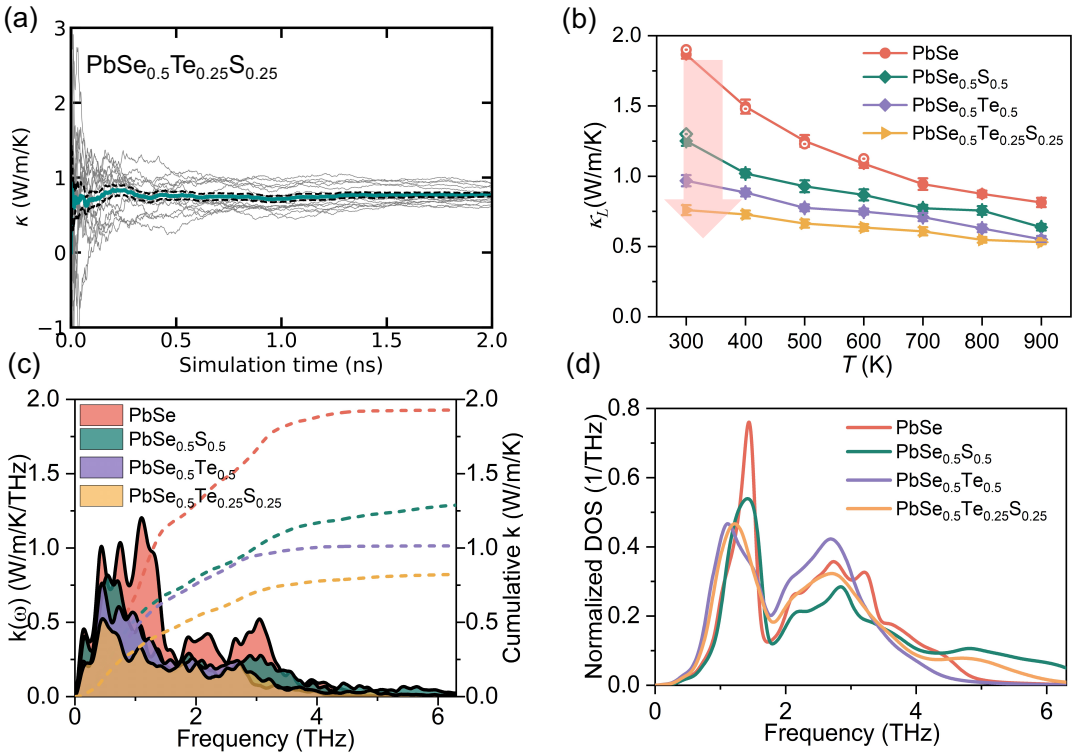

Figure 2 (a) Cumulative averages of the lattice thermal conductivity as a function of time calculated from HNEMD simulations for $PbSe_{0.5}Te_{0.25}S_{0.25}$ at 300 K using the NEP. (b) Lattice thermal conductivities of PbSe, $PbSe_{0.5}Te_{0.5}$, $PbSe_{0.5}S_{0.5}$ and $PbSe_{0.5}Te_{0.25}S_{0.25}$ at elevated temperatures. Hollow data points are taken from ref. [22]; points with the same color refer to the same system. (c) Spectral lattice thermal conductivities $k(\omega)$ (left axis) and the cumulative values (right axis) calculated from HNEMD. (d) Normalized phonon density of state (DOS) at 300 K.

We next study the lattice dynamics by performing Fourier transform of the velocity auto-correlation function [27] to obtain the normalized phonon vibrational density of state (DOS), as presented in Figure 2(d). The pronounced phonon peaks for PbSe and $PbSe_{0.5}S_{0.5}$ are located at around 1.4 THz, while the corresponding peak shifts left for the other two systems. At high frequency range (above 5 THz), $PbSe_{0.5}S_{0.5}$ has the highest phonon DOS, followed by $PbSe_{0.5}Te_{0.25}S_{0.25}$, due to the addition of light-weight S, consistent with the spectral thermal conductivity analysis.

Local chemical ordering has been discovered in high/medium entropy alloy systems [15,16,28], however, this phenomenon is yet to be further studied in thermoelectric materials. Here, we conducted hybrid Monte Carlo / molecular dynamics (MC/MD) simulations as implemented in large-scale molecular dynamics massively parallel simulator (LAMMPS) package [29] based on the developed NEP to simulate the annealing process to generate LCO. The sample was equilibrated at the prescribed annealing temperature for 40 ps under the NPT ensemble after energy minimization, followed by the hybrid MC/MD procedure, where random exchanges of S, Se, and Te atoms were attempted based on the Metropolis algorithm [30]. Two MD relaxation steps were conducted after one MC swap attempt. The energy-converged configuration was then cooled to 0 K for further MD simulations. As shown in Figure 3(a), the potential energy exhibits a decreasing trend during the process of swap attempts, indicating that a fully randomized state (maximum entropy) is energetically unfavorable with Te and S alloying. The atomic configurations of a random sample and the annealed sample at 600 K are presented in Figure 3(c); no large-scale segregation or ordering can be observed directly.

The Warren-Cowley parameter [31] has been used in many studies [28,32,33] to measure the degree of LCO, which is defined as $\alpha_{\Delta r}^{ij} = \frac{P_{\Delta r}^{ij} - c_j}{\delta_{ij} - c_j}$, where $P_{\Delta r}^{ij}$ is the probability of finding a j-type atom around an i-type atom in the neighbor shell Δr; δ_{ij} is the Kronecker delta function, and c_j is the concentration of j-type atom. A near-zero

$\alpha^{ij}_{\Delta r_{ij}}$ represents a random solid solution; a positive $\alpha^{ij}_{\Delta r}$ for the same element pairs ($i = j$) shows segregation; negative values for different species pairs suggest cluster ordering of the two elements. In this study, we calculate the LCO parameters in the second nearest neighbor (2NN) shells ($\Delta r_{ij} = 3.5 - 5$ Å) to describe the local chemical ordering in PbSe-based thermoelectric materials, as exhibited in Figure 3(b). Except the near-zero values for the random sample, the positive values of $\alpha^{Te-Te}_{\Delta r=3.5-5\text{ Å}}$ for the annealed $PbSe_{0.5}Te_{0.25}S_{0.25}$ demonstrate that Te atoms tend to occupy the 2NN sites of Te atoms. Similar behavior is also observed for the Se-Se and S-S pairs with a less obvious trend. This is consistent with previous report [11] that the (200) peak of the X-ray diffraction (XRD) pattern splits into several peaks when the alloying content of S/Te increases to 0.25 in PbSe; the XRD results suggested local regions with different fractions of S, Se and Te. Moreover, the wide distribution of the pair separation distance in the second coordination shells in Figure 3(d) illustrates the local lattice distortion in $PbSe_{0.5}Te_{0.25}S_{0.25}$. A higher amplitude of the partial radial distribution function of the Te-Te pair after annealing indicates local Pb-Te atomic environment, a similar but less obvious trend is also found for the Se-Se and S-S atomic pairs.

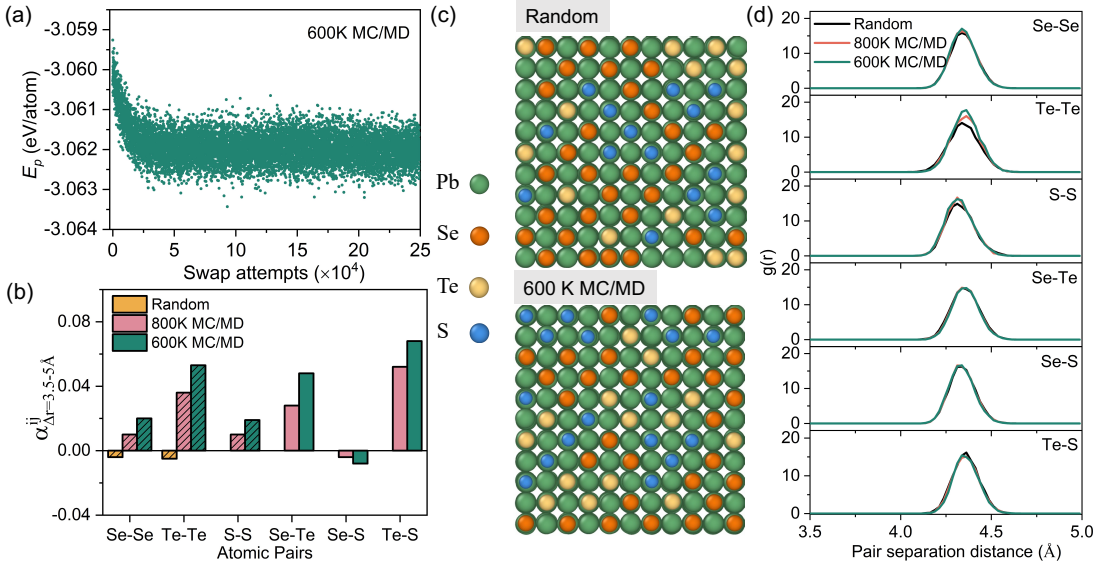

Figure 3. (a) Potential energy (E_p) variation with swap attempts during annealing at 600 K. (b) Second nearest neighbor (2NN) LCO parameters ($\alpha^{ij}_{\Delta r=3.5-5\text{Å}}$) for random and annealed $PbSe_{0.5}Te_{0.25}S_{0.25}$ samples (600 and 800 K). (c) Atomic distributions of random and 600 K annealed samples. (d) Partial radial

distribution functions $g(r)$ projected on Se-Se, Te-Te, S-S, Se-Te, Se-S, and Te-S atomic pairs of random and annealed $PbSe_{0.5}Te_{0.25}S_{0.25}$ samples.

Local chemical ordering in high/medium entropy alloys has been reported to affect the mechanical properties [28,33], but its influence on the thermal transport in entropy regulated systems is yet to be further studied. Here, we have calculated the lattice thermal conductivity of samples with and without local chemical ordering via HNEMD approach, as illustrated in Figure 4(a). The k_L at room temperature increases from 0.76 $Wm^{-1}K^{-1}$ for random $PbSe_{0.5}Te_{0.25}S_{0.25}$ to 0.87 $Wm^{-1}K^{-1}$ and 0.88 $Wm^{-1}K^{-1}$ for 800 K and 600 K annealed samples, respectively. The same trend can be observed in the whole temperature range from 300 K to 900 K. The increasing trend of k_L after the introduction of LCO can be further understood based on the spectrum of thermal conductivity $\kappa(\omega)$, as shown in Figure 4(b). Phonon modes with frequency in the range from 0 to 2 THz contribute dominantly to the thermal transport for both random and annealed samples. It is found that the contribution from phonon modes to k_L in the frequency range from 0 to 2 THz increases significantly in samples with LCO. Previous report [34] suggested that the anharmonic scattering rates of low frequency phonons can be reduced by LCO, leading to enhanced thermal transport. We find that the phonon density of states, as shown in Figure 4(c) has higher values for 800 K and 600 K annealed samples at frequency ranges from 0 to 1 THz and from 2 to 3 THz.

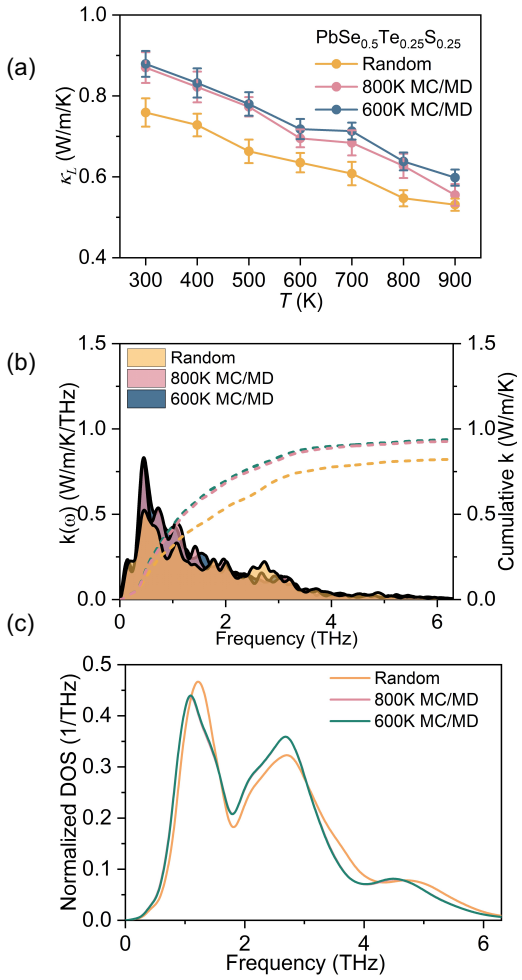

Figure 4. (a) Thermal conductivities of random, 800 K and 600 K annealed $PbSe_{0.5}Te_{0.25}S_{0.25}$ models at elevated temperatures. Error bars show the standard deviation. (b) Spectral thermal conductivity $\kappa(\omega)$ (left axis) and the cumulative thermal conductively (right axis) and (c) normalized phonon density of state (DOS) at 300 K for the random, 800 K and 600 K annealed models calculated from HNEMD.

In summary, the influences of entropy strategy and local chemical ordering on the lattice thermal conductivity of PbSe-based alloys are systematically investigated. The thermal conductivity decreases from 1.87 $Wm^{-1}K^{-1}$ of PbSe to 0.76 $Wm^{-1}K^{-1}$ when 50% of Se are substituted by Te and S. The local Te-Te ordering in the 2NN shell is discovered after hybrid MC/MD simulation, and the LCO enhances low frequency phonon contribution to the lattice thermal transport, resulting in about 14% increase of the lattice thermal conductivity. This work unveils the energy favorable LCO structure in $PbSe_{0.5}Te_{0.25}S_{0.25}$ and its effect on the thermal property, providing important

theoretical guidelines for engineering the thermal transport in entropy regulated thermoelectric systems.

Supplementary Material

The Supplementary material includes detailed information about density functional theory calculations, potential construction and validation, and convergence tests for molecular dynamics simulations.

Acknowledgements

This study is supported by the National Key Research and Development Program of China (2019YFA0209904) and the Research Grants Council of Hong Kong (C7002-22Y and 17318122). The authors are grateful for the research computing facilities offered by ITS, HKU.

Data availability

Data will be made available on request.

References

[1] B. Jiang, W. Wang, S. Liu, Y. Wang, C. Wang, Y. Chen, L. Xie, M. Huang, and J. He, Science **377**, 208 (2022).

[2] L.-D. Zhao, S.-H. Lo, Y. Zhang, H. Sun, G. Tan, C. Uher, C. Wolverton, V. P. Dravid, and M. G. Kanatzidis, nature **508**, 373 (2014).

[3] G. Tan, L.-D. Zhao, and M. G. Kanatzidis, Chemical reviews **116**, 12123 (2016).

[4] J. Mao, H. Zhu, Z. Ding, Z. Liu, G. A. Gamage, G. Chen, and Z. Ren, Science **365**, 495 (2019).

[5] Y. Pei, X. Shi, A. LaLonde, H. Wang, L. Chen, and G. J. Snyder, Nature **473**, 66 (2011).

[6] S. Lee, K. Esfarjani, T. Luo, J. Zhou, Z. Tian, and G. Chen, Nat Commun **5**, 3525 (2014).

[7] X. Qian, J. Zhou, and G. Chen, Nat Mater **20**, 1188 (2021).

[8] B. Jiang, Y. Yu, H. Chen, J. Cui, X. Liu, L. Xie, and J. He, Nat Commun **12**, 3234 (2021).

[9] C. Zhou and I. Chung, Coordination Chemistry Reviews **421**, 213437 (2020).

[10] Z. Chen, B. Ge, W. Li, S. Lin, J. Shen, Y. Chang, R. Hanus, G. J. Snyder, and Y. Pei, Nat Commun **8**, 13828 (2017).

[11] B. Jiang, Y. Yu, J. Cui, X. Liu, L. Xie, J. Liao, Q. Zhang, Y. Huang, S. Ning, B. Jia, B. Zhu, S. Bai, L. Chen, S. J. Pennycook, and J. He, Science **371**, 830 (2021).

[12] X. Su, P. Wei, H. Li, W. Liu, Y. Yan, P. Li, C. Su, C. Xie, W. Zhao, and P. Zhai, Advanced Materials **29**, 1602013 (2017).

[13] W. Li, S. Lyu, Y. Chen, and A. H. Ngan, Proceedings of the National Academy of Sciences **120**, e2209188120 (2023).

[14] S. Lyu, W. Li, Y. Xia, Y. Chen, and A. H. Ngan, Physical Review Materials **7**, 073602 (2023).

[15] S. Yin, Y. Zuo, A. Abu-Odeh, H. Zheng, X. G. Li, J. Ding, S. P. Ong, M. Asta, and R. O. Ritchie, Nat Commun **12**, 4873 (2021).

[16] X. Chen, Q. Wang, Z. Cheng, M. Zhu, H. Zhou, P. Jiang, L. Zhou, Q. Xue, F. Yuan, J. Zhu, X. Wu, and E. Ma, Nature **592**, 712 (2021).

[17] L. Zhou, Q. Wang, J. Wang, X. Chen, P. Jiang, H. Zhou, F. Yuan, X. Wu, Z. Cheng, and E. Ma, Acta Materialia **224** (2022).

[18] Z. Fan, Z. Zeng, C. Zhang, Y. Wang, K. Song, H. Dong, Y. Chen, and T. Ala-Nissila, Physical Review B **104** (2021).

[19] Z. Fan, W. Chen, V. Vierimaa, and A. Harju, Computer Physics Communications **218**, 10 (2017).

[20] Z. Fan, Y. Wang, P. Ying, K. Song, J. Wang, Y. Wang, Z. Zeng, K. Xu, E. Lindgren, and J. M. Rahm, The Journal of Chemical Physics **157** (2022).

[21] G. Akhmedova and D. S. Abdinov, Inorganic Materials **45**, 854 (2009).

[22] J. L. Wang, H. Wang, G. J. Snyder, X. Zhang, Z. H. Ni, and Y. F. Chen, Journal of Physics D: Applied Physics **46** (2013).

[23] Z. Fan, H. Dong, A. Harju, and T. Ala-Nissila, Physical Review B **99** (2019).

[24] T. Ghosh, M. Dutta, D. Sarkar, and K. Biswas, J Am Chem Soc **144**, 10099 (2022).

[25] M. Samanta and K. Biswas, Journal of the American Chemical Society **139**, 9382 (2017).

[26] L. Xu, Y. Xiao, S. Wang, B. Cui, D. Wu, X. Ding, and L. D. Zhao, Nat Commun **13**, 6449 (2022).

[27] J. Dickey and A. Paskin, Physical Review **188**, 1407 (1969).

[28] Q. J. Li, H. Sheng, and E. Ma, Nat Commun **10**, 3563 (2019).

[29] S. Plimpton, Journal of Computational Physics **117**, 1 (1995).

[30] B. Sadigh, P. Erhart, A. Stukowski, A. Caro, E. Martinez, and L. Zepeda-Ruiz, Physical Review

B **85**, 184203 (2012).
[31] J. Cowley, Physical Review **77**, 669 (1950).
[32] W.-R. Jian, Z. Xie, S. Xu, Y. Su, X. Yao, and I. J. Beyerlein, Acta Materialia **199**, 352 (2020).
[33] Y. Xia, S. Lyu, W. Li, Y. Chen, and A. H. Ngan, International Journal of Plasticity **169**, 103719 (2023).
[34] C. H. Baker and P. M. Norris, Physical Review B **91** (2015).